PHYSICAL REVIEW D

PARTICLES AND FIELDS

THIRD SERIES, VOLUME 28, NUMBER 7 1 OCTOBER 1983

Measurement of low-energy elastic $\pi^{\pm}p$ differential cross sections

J. S. Frank, A. A. Browman, P. A. M. Gram, R. H. Heffner, K. A. Klare, R. E. Mischke, D. C. Moir, D. E. Nagle, J. M. Potter, R. P. Redwine,* and M. A. Yates

Los Alamos National Laboratory, Los Alamos, New Mexico 87545

(Received 31 May 1983; revised manuscript received 18 July 1983)

We have measured differential cross sections for both π^+p and π^-p elastic scattering at incident-pion kinetic energies of 30, 50, 70, and 90 MeV in the center-of-mass angular range between 50° and 150°. The experiment detected pions scattered from a liquid-hydrogen target with multiwire proportional chambers and scintillation-counter range telescopes. The relative accuracy of each angular distribution is better than 5%, while the absolute cross sections have uncertainties of 4% to 25%. Our results for the absolute cross section for π^+p scattering at 30 and 90 MeV are inconsistent with previous measurements. Our π^-p measurements comprise the first extensive set of precision differential cross sections below 90 MeV.

I. INTRODUCTION

Since the development of intense beams of pions at the three "meson factories" (LAMPF, SIN, and TRIUMF), the pool of data from pion-nucleon and pion-nucleus interactions has expanded enormously. One exception has been the area of low-energy (<100 MeV) pion-nucleon scattering. This is not because of lack of interest in the data. Better low-energy pion-nucleon data are needed to improve the determination of S- and P-wave pion-nucleon phase shifts. In turn these are needed as input to microscopic calculations of pion-nucleus interactions.[1] There is also significant interest in the pion-nucleon system itself and improved data will help distinguish between various approaches that have been used to describe this interaction.[2] Better data are also required to help resolve the discrepancy between experimental and theoretical values of the pion-nucleus σ term.[3]

Some data have been published that are relevant to this energy region.[4–7] Only one of these was a measurement of the πp elastic differential cross sections for both polarities and as a function of energy. This was the experiment of Bussey *et al.*,[6] which measured π^+p and π^-p scattering down to 90 MeV. A measurement of the π^+p interaction at low energies was performed by Bertin *et al.*,[7] who studied π^+p scattering in the energy range of 21 to 96 MeV.

We present here measurements of π^+p and π^-p scattering at energies between 30 and 90 MeV. Although the measurements of low-energy $\pi^{\pm}p$ differential cross sections were among the fundamental experiments that were to be done at the meson factories, ours is the first such measurement from one of these facilities. The relative lack of experimental progress is due primarily to the difficulty of the experiments, especially in establishing a precise absolute normalization for the differential scattering cross sections. Uncertainties in the knowledge of the incident pion flux, particularly in a low-energy beam with significant contaminants, and in the knowledge of the thickness of a hydrogen target make absolute normalization exceptionally challenging.

Our π^+p data are of higher statistical precision than those of Bertin *et al.* and the π^-p data comprise the first extensive set reported below 90 MeV. After describing the apparatus, the data set, and the analysis, we discuss the problems and sources of uncertainties in the angular distributions and the absolute cross sections. Finally, comparisons of our data with predictions from energy-dependent phase-shift fits to the pion-nucleon system are presented.

II. EXPERIMENTAL METHOD

This measurement of low-energy π^+p elastic differential cross sections was conducted at the low-energy pion (LEP) channel at the Clinton P. Anderson Meson Physics Facility (LAMPF). Incident pions were detected by a beam counter and were then scattered from a liquid-hydrogen (LH_2) target. The angular distribution of the scattered pions was measured by a system of multiwire proportional chambers (MWPC's) and scintillation counters. Observations were made with both pion charges at four incident energies: 30, 50, 70, and 90 MeV.

In this section, we describe the pion beam and the monitors used to measure its flux and composition, the LH_2 target and the apparatus used to measure its thickness, the scattering system, and the event trigger. A side view of the experiment is shown in Fig. 1.

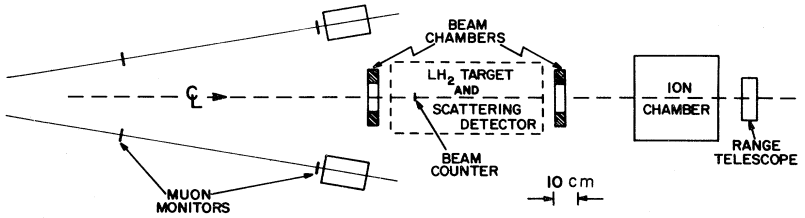

FIG. 1. Side view of the apparatus for the experiment showing the beam monitors.

A. Beam

1. Pion beam

The pions for this experiment were produced from the interactions of the 800-MeV proton beam at LAMPF within a 3-cm-thick graphite target. Collimators at the entrance of the LEP channel defined a small solid angle. This allowed the beam spot at the LH_2 target to be small in size and divergence. (See Table I for a summary of beam parameters.) The central pion energy was known from measurement of the fields of the bending magnets to better than 0.1%.

The trigger rate in the scattering apparatus was limited to about 10/s by adjusting the momentum slits. The average beam flux ranged from 10^5 to 10^6 particles/s. The duty factor of the beam was 6%, so instantaneous rates were 16 times higher. Pions comprised 30% to 90% of the total flux, depending on the energy and polarity of the beam.

During most of the experiment, the channel was set for a normal point-to-point achromatic focus. At 30 MeV, observations were also made with a 234-mg/cm^2 CH_2 degrader placed in the middle of the channel, where there is a crossover in the bend plane, to help separate electrons from pions by differential energy loss. This reduced the electron contamination by about a factor of three.

2. Beam chambers

The beam characteristics at the center of the target were obtained by measurements made with MWPC's in the beam, one upstream of the LH_2 target and one downstream. Each chamber recorded the horizontal and vertical positions of a traversing particle to a precision of 2 mm (full width). This allowed measurement of the beam size and divergence and extrapolation of beam trajectories into the target region. The horizontal and vertical beam sizes and divergences at the target were found to be approximately the same.

B. Beam monitors

1. Beam counter

The beam counter was a fast scintillator 0.16-cm thick and 4.76 cm in diameter viewed by a high-gain fast phototube 5 cm in diameter. This counter, located 26 cm upstream of the target, defined the particles that traversed the target, thereby eliminating from consideration a large part of the muon halo that accompanied the pion beam. The primary measurement of the incident flux of particles was made by scaling pulses from this counter.

2. Split-foil ionization chamber

An ionization chamber, located 70 cm downstream of the H_2 target, measured the total beam flux that passed through the apparatus. It was divided into three sections: two provided redundant measurements of the total beam flux and a third was split into horizontal and vertical segments to detect beam motion. The segmented chamber proved quite useful as an aid to rapid alignment of the vertical position of the beam when conditions were changed.

TABLE I. Beam parameters and data sets for this experiment.

T_π nominal (MeV)	Polarity	Beam tune	T_π target center (MeV)	Full width (MeV)	Spot size σ (cm)	Divergence σ (mr)
90	+	Normal	89.6	0.1	0.7	15
90	−	Normal	89.6	0.4	0.7	15
70	+	Normal	69.6	0.1	0.9	20
70	−	Normal	69.6	0.7	0.9	20
50	+	Normal	49.5	0.1	1.1	25
50	−	Normal	49.5	0.9	1.1	25
30	+	Normal	29.4	0.4	1.1	25
30	+	Degrader	29.4	0.4	1.1	25
30	−	Degrader	29.4	0.6	1.1	25
30	−	Degrader, double intensity	29.4	0.6	1.1	25

3. *Muon monitors*

Two scintillation-counter telescopes monitored the pion flux by detecting muons from $\pi \rightarrow \mu\nu$ decay. Each telescope consisted of two small scintillators that defined a region of position and angle with respect to the beam and a thick counter that measured the total energy of the particle that passed through the smaller scintillators. These two telescopes were mounted, one above the beam line and one below, so sensitivity to beam motion in the vertical direction, which is the bend plane of the channel, could be canceled. The geometry was set to pick out $\pi \rightarrow \mu\nu$ decays from a vacuum region upstream of the experiment with decay angles smaller than those of the Jacobian peak. The pulse-height distribution recorded from the thick scintillator for the 50- and 70-MeV runs displayed two distinct energy peaks that corresponded to the two muon energies that occur at a given angle inside the Jacobian peak. At 30 MeV, muons in the low-energy peak were stopped before reaching the thick counter. At 90 MeV, the angle of the monitor overlapped the Jacobian angle so only one energy peak was resolved.

C. H_2 target and thickness monitors

1. *LH_2 target*

Liquid hydrogen was contained in a cylindrical target cell 20 cm in diameter and nominally 1.44 cm in length. The liquid cell, which had very thin end windows (3.3 mg/cm^2 Mylar), was located at the center of a spherical ballast vessel 28 cm in diameter with 28-mg/cm^2 Mylar windows. This vessel in turn was centered within a vacuum container with 33-mg/cm^2 Mylar windows. As shown in Fig. 2, the axis of the target was in the scattering plane and was rotated to an angle of $(45.0 \pm 0.1)°$ with respect to the beam. The H_2 gas in the ballast vessel was maintained at the same pressure as the vapor above the liquid in the target cell by a direct connection. Therefore, the thin windows of the cell felt only the pressure differential due to the hydrostatic load of the LH_2 in the reservoir and in the cell itself. Optical surveys revealed that the inner windows bulged significantly under this stress.

Hydrogen gas was liquified from a closed system by a 10-W refrigerator. By keeping the quantity of H_2 in the system constant, it was possible to ensure that the amount of liquid in the target and reservoir remained constant and that consequently the bulge of the target cell was reproduced each time the target was refilled.

The density of the LH_2 was determined by measuring the vapor pressure to a precision of 0.1 psia. From this measurement, the density of the liquid was determined to 0.05%. A semiautomatic regulator maintained the temperature of the LH_2 at a constant value by supplying heat to the system as required to offset the constant cooling of the refrigerator. Silicon-diode thermometers measured the temperature of the ballast gas at two distances from the liquid cell to determine the temperature gradient in the H_2 gas.

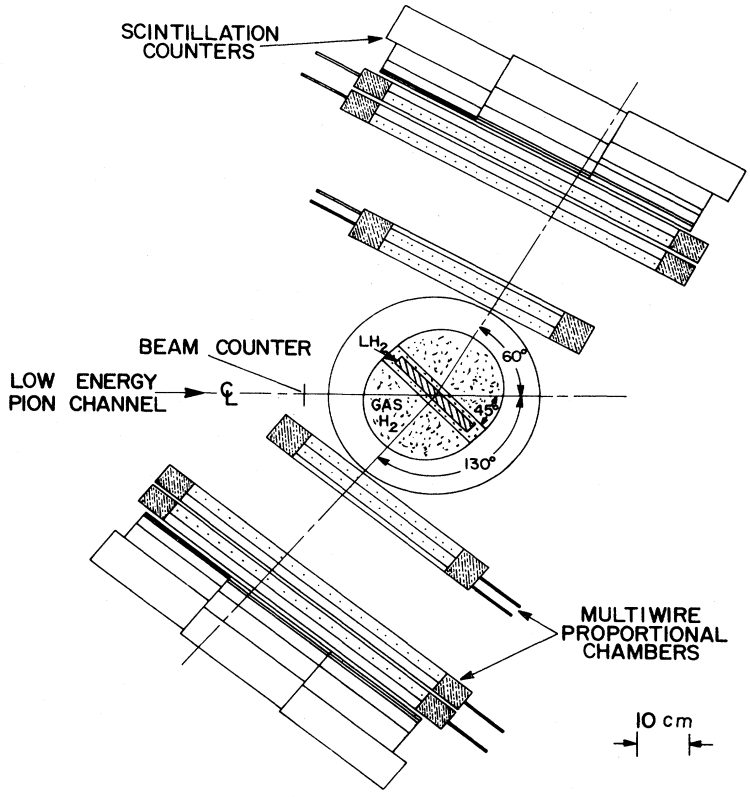

FIG. 2. Top view of the scattering detector and the H_2 target.

2. Range telescope

A counter telescope of seven thin scintillators was placed downstream of the ionization chamber. The counters were 0.127-cm thick and were individually wrapped; each constituted a thickness increment of 0.184 g/cm^2. A differential range method utilized these counters to measure the thickness of the H_2 target.

D. Detector

Scattered pions were detected by two nearly identical arrays of MWPC's and scintillator telescopes located on either side of the beam (see Fig. 2). The forward-angle detector covered the laboratory angular range from 38° to 97°, the backward-angle detector covered the range from 95° to 152°. Overlapping measurements were provided by rotating the forward-angle detector back by 10° and the backward-angle detector forward by 10°. For each array, the azimuthal acceptance of the apparatus was approximately 5%.

1. MWPC arrays

Each array presented four horizontal (x) and four vertical (y) wire planes to the scattered particles; the front and rear pairs of planes were separated by 25 cm. The MWPC's had 20-μm gold-coated tungsten sense wires spaced 2 mm apart and were equipped with an individual-wire readout system (PCOS II).[8] The use of four MWPC's permitted continuous monitoring of individual chamber efficiencies using the experimental data itself. The trajectory of a scattered particle was determined with three or more measurements of x and y even in the presence of multiple tracks. The angle of a trajectory with respect to the nominal beam line was determined to ± 12 mrad. This uncertainty in the scattering angle was smaller then the uncertainty introduced by the phase space of the incident beam.

2. Scintillation counters

The MWPC arrays on each side were followed by three adjacent scintillator telescopes (six in all). These telescopes consisted of five or, for the most forward set, six counters. Each counter had a folded light guide which ended at a phototube on the top side. The thicknesses of the counters were carefully chosen to give range information for the pions. In each telescope the first two counters were traversed by the elastically scattered pions at all of the incident energies. They were part of the event trigger logic and also served to measure energy loss (dE/dx). The third counter just stopped the pions that had 30-MeV incident energy before scattering to that particular angle; the fourth measured the range of scattered 50-MeV pions and so on. In the five-counter telescopes, 70- and 90-MeV pions were treated together. Range information as well as dE/dx and the total deposited energy, E, aided in identifying pions and rejecting muons and electrons, which at a given beam momentum generally had greater range than pions. Muons from pion decay in the space between the end of the channel and the target had a spread of momenta that precluded their rejection by range criteria alone but these were efficiently rejected by observing both dE/dx and E.

E. Trigger

Details of the electronic logic will not be given here; only the operating precepts will be described. The trigger logic identified potentially interesting scattered particles by establishing a fast coincidence between a signal in the beam counter and in one of the six counter telescopes. A counter telescope, in turn, triggered on a particle if there was a fast coincidence between the first three counters. The occurrence of this event trigger plus a requirement from the MWPC's caused the data-acquisition logic to be disabled while a variety of data were recorded. First, the pattern of all of the counters that had recorded the passage of a particle was entered into an array of latch circuits. Similarly, the pulse from each counter was gated into an analog-to-digital converter (ADC), and pulses were sent to the stop inputs of an array of time-to-digital converters (TDC's) whose common-start input was derived from the event trigger. The event trigger also caused the PCOS system to begin the readout of the addresses of the struck wires.

An important feature of the electronics prevented the flux of muons from the decay $\pi \rightarrow \mu\nu$ from overwhelming the signal from scattered pions. An off-line trajectory projection could have been used to eliminate all but the relatively small number of muons born in the target itself, but all events would first have been accepted by the logic and then recorded on magnetic tape. This procedure would have been wasteful of both data-taking time, owing to the dead time it would have caused, and later, of analysis time. To eliminate the bulk of these unwanted events a special purpose hard-wired logic system was built that performed a very crude track reconstruction.[9] This logic decided within about 0.5 μs whether or not a track originated in a region acceptably close to the target. This circuit used the "dc latch outputs" provided for each wire by the readout system to "reconstruct tracks" merely by establishing coincidences between appropriately chosen groups of wires in each of the spatially separated wire planes.

Obviously, such a hard-wired logic circuit was very inflexible; to guard against irretrievable rejection of good data the limits of acceptance were made permissive. Normally the coordinates in any three out of four chambers were required to fulfill the coincidence requirement, but runs were made in which these criteria were relaxed in differing patterns. Intercomparison of these data revealed that $>97\%$ of the tracks originating in the target were accepted in all cases. The rejection of useless events achieved by the standard logic requirement of "three out of four" was better than ten to one compared to "no restriction." If the hard-wire track reconstruction logic was not satisfied that a potentially useful track was present, an "abort analysis" pulse was issued that stopped the readout and re-enabled the logic to proceed with data acquisition. When a potentially useful track was seen, the conversion of wire addresses was allowed to proceed and, when comp-

leted, the data from latches, ADC's and TDC's was read and written to magnetic tape as a sequence of words describing a single event. Appropriate circuitry kept track of the computer and electronic dead times. Information from various monitors and scalars was also recorded on tape every 100 s and at the end of each run.

III. DATA COLLECTION AND ANALYSIS

Several types of data were acquired to self-calibrate the performance of the apparatus so corrections applied to the cross-section measurements were well determined. They may be grouped into three categories: calibration of the scintillation counters, trigger-efficiency studies, and beam and target calibration measurements. The special runs that were made to study the beam and target are discussed in the normalization section. The runs that checked the efficiency of the trigger are discussed in the results section. We discuss the scintillation-counter calibration runs below. Then the normal data collection and analysis procedure are described.

A. Data

1. Scintillation-counter calibration

The corrections necessary to account for nuclear interactions that occurred in the banks of scintillators were directly measured by the scintillators themselves in a series of special runs. The main proton beam was chopped into short bursts that struck the pion production target approximately 1500 times per second. This permitted measurement of the time of flight (TOF) for each particle between the production target and the apparatus. Individual groups of counters were rotated into the beam and each incident particle was identified by its timing. For these runs, the beam momenta were adjusted to correspond to the energies of the scattered pions that the counters detected when they were in their nominal positions for normal data collection. Figure 3 shows the probability that a tagged π^-, μ^-, or e^- with 170-MeV/c beam momentum (T_π=80 MeV) penetrated 49 mm of scintillator and registered in the next counter. Runs of this type were made for both polarities, and several incident momenta, for most of the counter banks.

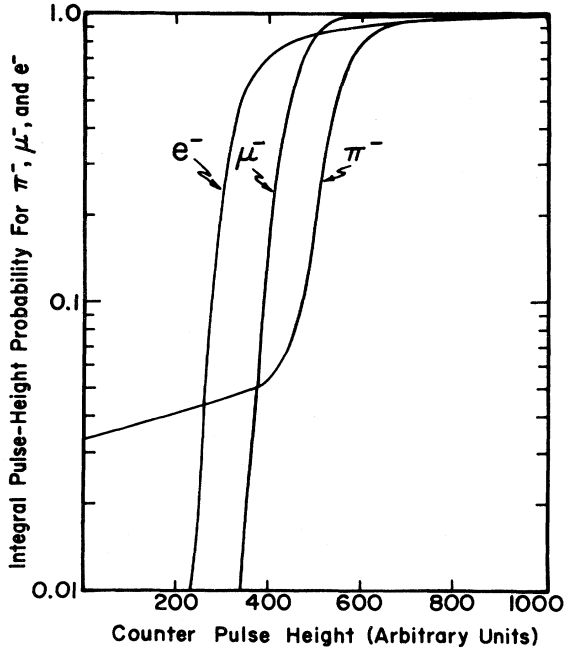

FIG. 3. Experimentally determined probability distribution that a 170-MeV/c π^-, μ^-, or e^- penetrated 49 mm of scintillation material and registered a pulse in the next counter.

We found that the loss due to requiring that a particle penetrate a given distance ranged from 1.0%/cm for 80-MeV π^+ to 2.0%/cm for 20-MeV π^+. The corrections for π^- were well described by 1.2 times the π^+ correction. The reason higher-energy particles have a smaller loss of detection efficiency in spite of a larger interaction cross section is that they tend to produce higher-energy interaction products that continue to penetrate through the scintillation material. The typical corrections for these nuclear interactions were 2% to 5% and are summarized in Table II. The errors represent the systematic uncertainties for each counter bank; they are highly correlated.

TABLE II. Interaction corrections for the six counter banks.

T_π (MeV)	Polarity	Counter bank: Left Front	Left Middle	Left Back	Right Front	Right Middle	Right Back
		(%)					
90	+	1.7±0.5	1.1±0.4	1.0±0.4	0.9±0.4	0.6±0.3	0.4±0.3
90	−	2.0±0.6	1.3±0.5	1.2±0.4	1.1±0.4	0.7±0.4	0.5±0.3
70	+	2.2±0.5	2.0±0.6	1.8±0.7	1.5±0.6	1.1±0.6	0.8±0.6
70	−	2.8±0.5	2.5±0.6	2.2±0.7	1.9±0.6	1.3±0.6	1.0±0.6
50	+	3.1±0.7	2.5±0.9	2.0±0.7	2.0±0.7	1.5±0.7	1.0±0.5
50	−	3.7±0.8	3.0±1.1	2.4±0.8	2.4±0.8	1.8±0.8	1.3±0.6
30	+	4.5±2.2	3.7±1.8	3.0±1.5	3.0±1.5	2.4±1.2	1.7±0.9
30	−	5.7±2.8	5.2±2.6	4.2±2.1	4.2±2.1	3.4±1.7	2.5±1.3

2. Beam profile and composition data

At each beam energy and polarity, a series of runs was performed to determine the beam characteristics. This included measurements of the beam spot and divergence with the beam chambers and measurements of the beam composition with the beam counter.

3. Scattered-pion data set

The data taken to determine the angular distribution of scattered pions was composed of ~ 10 to 20 separate runs at each energy and polarity. Each of the target-full runs typically had from 10^3 to 10^4 scattered pion events. Approximately $\frac{1}{4}$ to $\frac{1}{3}$ of the data-taking time was used for target-empty runs so the statistical accuracy of the scattered pion signal was not dominated by the subtraction. The scattering apparatus was rotated by 10° as described previously, and another complete set of target-full and target-empty runs was taken.

At 30 MeV, runs were taken with two different beam conditions for both π^+ and π^- beams. For 30-MeV $\pi^+ p$ measurements, data were taken with both the normal beam tune and with the degrader in the beam (Sec. II A 1) to check that the results were not sensitive to differing beam conditions. For the 30-MeV $\pi^- p$ measurements, data were taken with two different settings of the LEP collimators that set the channel solid angle. This resulted in a change in pion flux by about a factor of 2 and served to check the sensitivity of the results to beam intensity.

B. Analysis of angular distributions

The analysis of the scattered pion data proceeded in several stages. The first-pass analysis eliminated those events that had pulse heights incompatible with the detection of a scattered pion, had a track that projected outside of a fiducial region within the gas envelope of the H_2 target, or had too little or too much information from the wire chambers. Any event that could possibly be a scattered pion from near the liquid region of the target was retained.

A refined set of parameters for the algorithms used to fit pulse-height spectra and to convert MWPC coordinates to tracks in space was derived from this first replay. With these parameters the final pulse-height and geometric criteria that defined πp elastic scattering events were established. A second replay of all the data using these criteria produced the data set that was reduced to cross sections. Target-empty backgrounds were then subtracted from the target-full data as a function of scattering angle. The final angular distributions were obtained by combining the results from the two different detector rotations. We now discuss the event selection procedures in greater detail.

1. Wire-chamber information

If a particle registered in all four wire chambers that made up each array, four x and y coordinates were produced. These coordinates were fitted by a least-squares method to straight lines. To be retained for analysis a track had to have at least three of the four coordinates fall acceptably close to a straight line in both projections. Fiducial regions were defined 8 mm inside the frames of all of the wire chambers to reduce the reconstruction sensitivity to MWPC performance near edges. Typical chamber efficiencies were greater than 98%/plane. Generally more than 90% of the events had unique reconstructible tracks in both the horizontal and vertical chamber coordinates. Most of the rest of the events had two candidate tracks. Some of these had well-separated distinct tracks that came within the live time of the chamber encoding system; others came from a process such as $\pi \to \mu\nu$ decay in which a single track with a kink was reconstructed as two tracks.

The reconstructed trajectories were first used to project back to the beam line to eliminate events that did not originate from within ± 5 cm of the LH_2 target. Figure 4 shows the resulting projection of some 30-MeV π^+ data for backward scattered particles. The vacuum and gas windows are clearly resolved. The dashed line results from the corresponding target-empty run normalized to an equal number of incident pions.

The tracks were also projected forward into the banks of scintillation counters. This allowed definition of a geometrical region within each counter bank that was not influenced by possible inefficiencies near the physical edges of the counters.

2. Scintillation-counter analysis

The pulse-height and range information from the counter stacks provided redundant information to identify

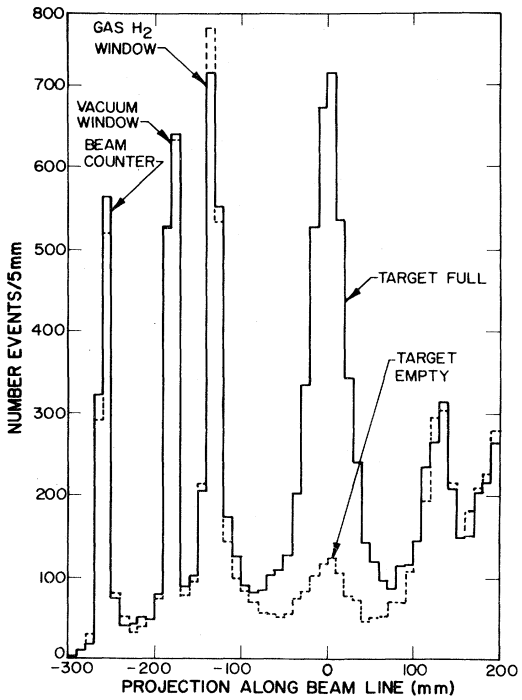

FIG. 4. Track reconstruction of backward-scattered-π^+ data at 30 MeV. The liquid region, the beam counter, and the four outer windows of the H_2 target assembly are clearly resolved. The dashed line shows target-empty data normalized to the same flux of incident particles.

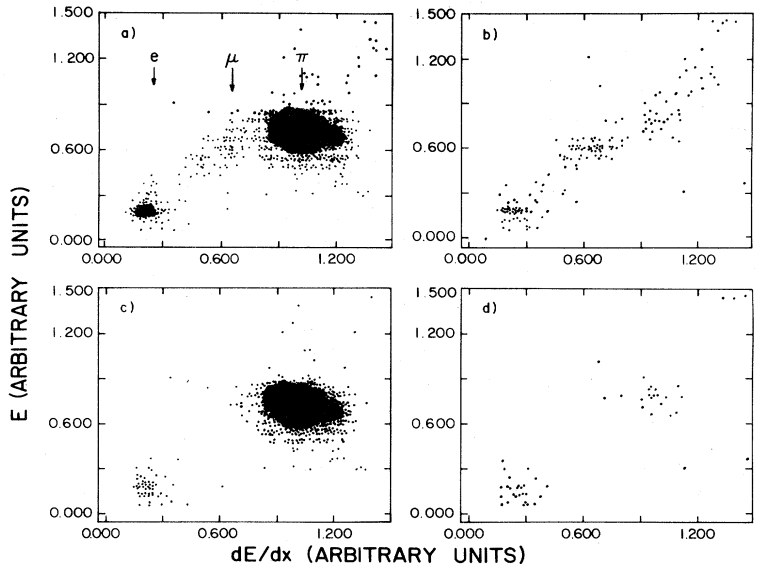

FIG. 5. E versus dE/dx plots for backward-scattered-π^+ data at 30 MeV. Both (a) target-full and (b) target-empty data are shown. Cuts have been made that eliminate events that do not originate from the target. Most electrons have also been eliminated. Shown in (c) and (d) is the effect of demanding that the counter behind the calculated stopping counter has little or no pulse.

pions and eliminate other particles efficiently. This apparent overdetermination of the signature of a scattered pion was quite important in determining the best possible criteria for identifying stopping π^-, for which the total measured energy and, at some level, the range information is rendered useless due to nuclear processes that take place at the end of their range. Figure 5 shows E versus dE/dx plots for some 30-MeV π^+ scattering data in the backward hemisphere. The π, μ, and e components are readily observed. Also shown are the pulse-height plots that were obtained when a range cut was applied by demanding a small or zero pulse height in the next counter beyond the one in which the pion should have stopped. Muon and electron backgrounds become very apparent with this technique.

Since a relatively large fraction of the higher-energy pions interacted within the scintillator material before stopping, the pulse-height cuts were applied to counters as near the front of the counter stack as feasible to minimize corrections for lost pions. The dE/dx in each counter was corrected for the experimentally determined pulse-height attenuation by using MWPC track information projected into the counter. Any particle that had a corrected dE/dx greater than a specified minimum was accepted as a pion. The calibration data, which gave the response of each counter stack to pions, demonstrated that a cut with a lower bound only reduced the efficiency differences between π^- and π^+ to a very low level. For the 90-MeV data no dE/dx cuts were applied, since the discrimination between pions and electrons was poor in the first two counters and a relatively large correction for interactions would have been required if cuts were imposed on dE/dx in the thicker counters. Determination of the systematics of the energy cuts from pions being lost and from nonpion backgrounds being included were determined by using all the information from the counter stacks and from the calibration runs.

3. *Target-full and target-empty comparison*

After the MWPC and scintillator information had been used to eliminate events that were not consistent with πp elastic scattering, the remaining events were either scattered pions or background events that came from the target region and had pulse-height information compatible with scattered pions. The target-empty subtraction eliminated most background events that could not otherwise be eliminated. The ratio of net signal to target-empty background as a function of scattering angle is given in Table III.

4. *Backgrounds*

Even after all cuts were applied, the net signal still had target-associated backgrounds. The most difficult background to eliminate arose from the charge-exchange reaction, $\pi^-p \rightarrow \pi^0 n$, followed by Dalitz decay or photon con-

TABLE III. Ratio of elastic πp signal to target-empty background as a function of center-of-mass angle.

T_π (MeV)	Polarity	$\theta^{\text{c.m.}}$ 50°	100°	150°
90	+	8.4	17.8	16.8
90	−	4.7	1.6	1.4
70	+	6.2	19.8	21.2
70	−	4.5	3.1	0.4
50	+	4.3	17.2	17.0
50	−	4.8	1.7	1.0
30	+	5.2	12.5	12.2
30	−	8.7	6.3	2.2

version in the target. This was an important background since at most of our energies the charge-exchange cross section is more than a factor of 10 larger than the elastic cross section at backward scattering angles. Figure 6 shows the ratio of the observed to predicted pulse height in the fourth counter of the stack that detected the most backward scattered pions at 90-MeV beam energy. The plotted data are the target associated $\pi^- p$ scattering. The curve that is drawn for the pion signal was the observed spectrum from $\pi^+ p$ scattering in this counter at the same scattering angles. The electron curve was determined from the calibration runs. From these data, we determined that $(18\pm4)\%$ of the total target-associated signal at these angles was not consistent with elastic $\pi^- p$ scattering.

In addition to a net signal from the charge-exchange reaction, there was also a small electron net signal from two other sources. The first of these gave electrons at forward angles due to electromagnetic interactions. The second source of electrons was isotropic and random in time as expected from decays of muons stopped within the target.

From examination of the pulse-height distributions in counters behind those in which the pulse-height cuts were placed and from the TDC distributions of the trigger counters, corrections or upper limits were derived for the number of non-πp elastic events that were included in the final data set. Evidence for a net signal from electrons was found only for the $\pi^- p$ data at 70 and 90 MeV; corrections of greater than 0.2% were necessary only for the 90-MeV data set. For other energy and beam-polarity combinations, a systematic uncertainty for the possible electron contamination has been included. The systematic errors for these effects are generally less than 1% for the π^+ data and up to 4% for large angles in the π^- data.

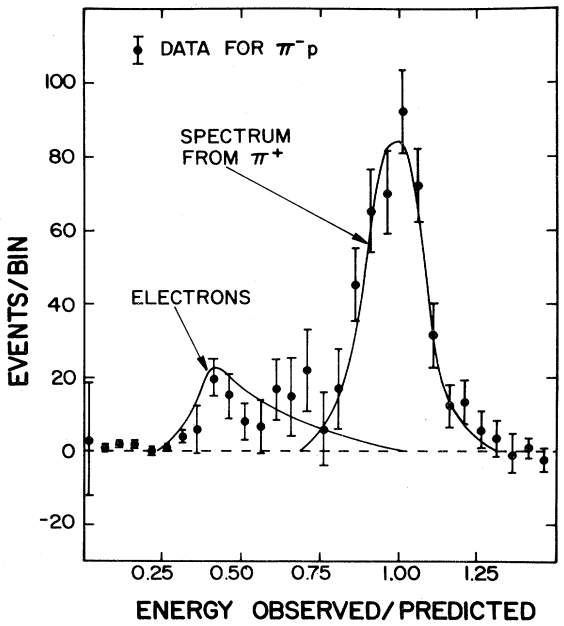

FIG. 6. The ratio of the observed to predicted pulse height of the net signal in the fourth counter in the stack that detected the most backward set of scattering angles for 90-MeV beam energy. The curve drawn for the pion signal was the observed spectrum for $\pi^+ p$ scattering in this counter at the same scattering angles. The curve for electrons was determined from the calibration runs.

Since the Mylar that held the LH_2 consisted of C and O nuclei in addition to H, pions scattered elastically and inelastically from these nuclei were detected by our apparatus. Few of these were eliminated by the dE/dx cuts. To first order, the contribution from these processes was eliminated by the target-empty subtraction. However, since the energy of the pion changed significantly when it passed through the LH_2 and the various nuclear cross sections are energy dependent, the subtraction technique had a systematic uncertainty. For this, we estimate that the change in the target-wall background is less than 0.9% at 30 MeV to 0.6% at 90 MeV. The uncertainties due to this effect are included in the angular-distribution systematic errors.

5. *Nonanalyzable events*

The analysis program rejected certain classes of events that were too complicated, had too little information to determine the scattering angle, or had more than one track. Typically 90% of the events on tape were analyzable. There was no target-associated signal in any class of rejected events except the catagory of more than one track in the wire chambers.

The correction for these nonunique events was determined for forward and backward scattering angles and ranged from 2 to 3% for all π^+ scattering data. For the π^- data sets, the beam intensity was typically higher than for the π^+ data, and the correction was between 3 to 4.5%. The systematic uncertainty was taken to be 25% of the correction. The angular distribution of these events was consistent with the angular distribution of the scattered-pion signal of the π^+ data; therefore this systematic error was included in the normalization uncertainty. In addition to this overall correction factor, events from $\pi^- p$ in the backward direction that had more than one track were found to be consistent with charge exchange and subsequent Dalitz decay or photon conversion for which two electrons passed through the chambers. Events that were consistent with electron pairs formed up to 20% of the net signal for backward-angle 70-MeV $\pi^- p$ data and up to 10% at 50 MeV. These events were not added back into the elastic-scattering differential cross section.

C. Normalization of data set

The conversion of the observed number of pions that elastically scattered from protons as a function of angle into differential cross sections requires knowledge of the absolute acceptance of the apparatus, accurate determination of the pion beam flux to which the apparatus was sensitive, and the effective number of protons in the target. We now discuss these factors.

1. *Monte Carlo acceptance calculation*

A Monte Carlo method was used to calculate the acceptance of the apparatus. Included in the simulation were

pion decay, multiple scattering, chamber resolution, and energy loss in scintillator material. The simulation followed an incoming pion, allowed it to scatter isotropically in the target, and then traced it through the detectors. It simulated hits in the MWPC's and energy deposited in the scintillators. Resolution effects were included in the MWPC hit positions and in the counter pulse heights. The same track-fitting procedures, fiducial cuts, and pulse-height cuts were applied to the Monte Carlo events as were applied to the data.

Figure 7 shows the Monte Carlo results obtained for an isotropic angular distribution and the net signal for one rotation of a 30-MeV π^+p data set. The other rotation provided redundancy and reduced the sensitivity to the uncertain acceptance at the counter edges. From extrapolation of the chamber data back to the target, we find that the position of the center of the target was uncertain to ± 2 mm. This 2-mm uncertainty leads to two effects. One is that the solid angle of the experiment may have a 0.6% bias between forward and backward scattering angles. This represents a systematic uncertainty of $\pm 0.6\%$ for forward scattering angles, and a $\mp 0.6\%$ systematic uncertainty for backward scattering angles.

The second effect involves the detailed matching of the counter fiducial area cuts between the data and the Monte Carlo simulation. Although the acceptance calculation matches the pattern of rise and fall of the data quite well as can be seen in Fig. 7, the 2-mm uncertainty leads to an uncertainty of 0.5° in scattering angle. This uncertainty results in corrections of opposite sign on each side of the six sets of counters. To good approximation this error is well represented by an uncertainty in the rate of fall in the acceptance near the counter edges. The error in the calculated acceptance was increased near the counter boundaries to account for this effect.

2. *Number of pions*

The number of incident pions was obtained by scaling the total flux seen by the beam counter and multiplying it by the fraction of the beam that was pions (f_π). This fraction was determined by the same technique used for identifying particles in the calibration runs (Sec. III A 1). This permitted measurement of f_π without changing the pion channel settings. Figure 8(a) shows a typical TOF spectrum for the 50-MeV π^- beam with the electric field of the plates that provided the beam chopping set to normal polarity. However, this chopping field perturbed the location of the proton beam on the production target. We found that f_π was very sensitive to beam position. The number of pions per incident proton is not sensitive to small beam motions. However, the number of electrons, which come largely from π^0 decay and the subsequent conversion of the γ rays within the production target, is quite sensitive to the thickness of target available for conversion.

To determine the sensitivity of f_π to the chopping field, the polarity of the chopper was changed so that beam was swept in the opposite direction. Figure 8(b) shows the same 50 MeV, π^- beam, but with the chopper set to re-

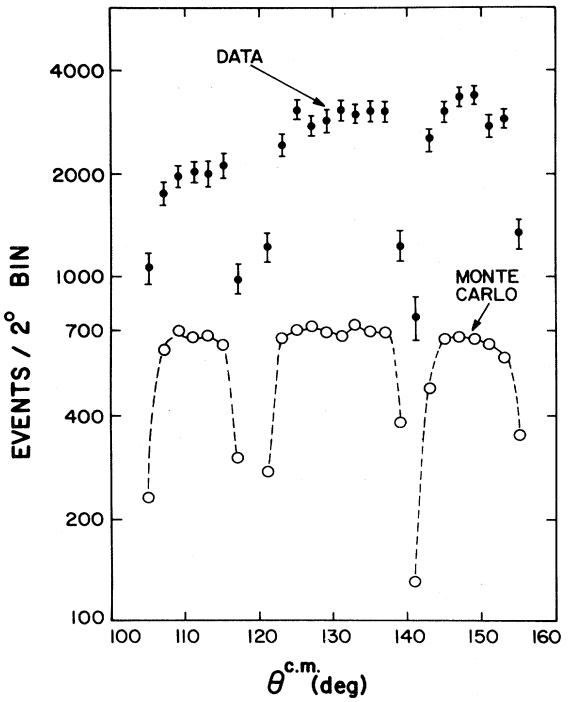

FIG. 7. Data and Monte Carlo angular distributions for backward-scattered 30-MeV π^+p data. The angular distribution of the Monte Carlo was isotropic. The other rotation set fills in the gaps in acceptance and provides redundancy.

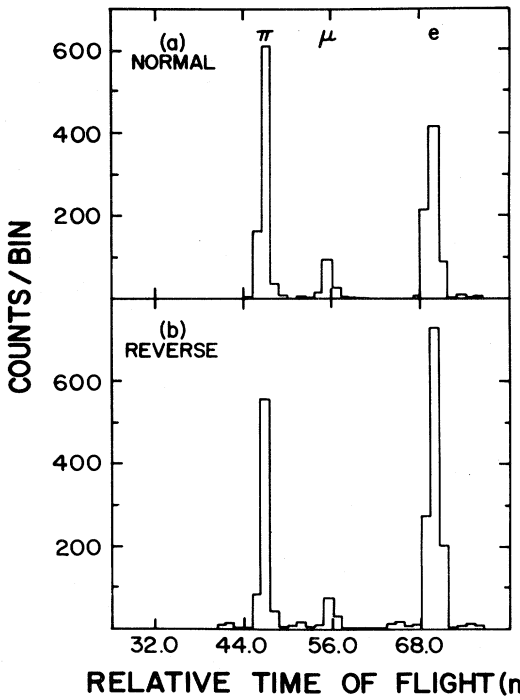

FIG. 8. Chopped-beam results for the 50-MeV π^- beam. Results for chopper in (a) normal polarity and (b) reversed polarity.

verse polarity. For normal chopper polarity at 50 MeV, $f_\pi = 0.482 \pm 0.020$; for reversed chopper polarity, $f_\pi = 0.339 \pm 0.013$. The errors are statistical uncertainties. Under running conditions f_π must have been between these two numbers, but we cannot determine its value more exactly.

We did not measure f_π with both polarities of the beam chopper for most of the 50-MeV and higher-energy data. We estimate the uncertainty here by noting that for normal beam parameters the number of electrons per pion no more than doubled when we changed from normal to reverse chopper operation. Since the polarity of the chopper was unknown when only one polarity was taken, we take the range of uncertainty to be bracketed by the f_π obtained when we either double or halve the e/π ratio. Table IV summarizes the measurements of f_π for our various running conditions and tabulates the values of f_π used in calculating cross sections.

The f_π obtained from the chopper data was checked for the 30-MeV π^+ beams and the 50-MeV π^- beam by looking at the pulse-height distribution from the beam counter. At these energies, the electron and pion energy losses were sufficiently different to allow extraction of a value of f_π from pulse-height spectra acquired under running conditions. The value of f_π obtained in this way for the normally tuned 30-MeV beam was 0.30 ± 0.02, which is consistent with the f_π for this condition using the average of normal and reverse chopper data. Good agreement between the two methods of determining f_π was also found with the midplane degrader in place at 30 MeV for both polarities. Pulse-height data for production runs at other energies were not recorded, so other determinations of f_π could not be verified in the same manner.

Several corrections were made to f_π before the number of pions striking the target was determined. The first one was for the particles in the calibration runs that had the TOF of a pion but that were actually arising from pions decaying just upstream of the beam counter. This correction reduced f_π by 1.3 to 1.6%. The second correction accounted for those pions that decayed in the 26 cm between the beam counter and the target. At 90 MeV, 2.5% of the pions decayed in this region; at 30 MeV, 4.7% decayed. Interactions in the beam counter and in the material upstream of the liquid cell reduced the pion flux by only 0.2 to 0.7%. These correction factors were combined and are summarized in Table IV.

The muon monitor could not be used as an absolute monitor of the pion flux because the telescopes pointed upstream to a decay region that was partially inside the last quadrupole magnet in the LEP channel. This made the muon monitor quite sensitive to the phase space of the beam within the magnet. Also, while the trigger responded only to the flux of pions that passed through the beam counter, the muon telescopes detected decay muons from within the entire beam phase space. Therefore the muon counters provided only a relative measurement of the incident pion flux. As relative monitors, the muon telescopes performed well. The ratio of counts in these telescopes was typically stable to 1%, and the counts in them were highly correlated with the counts in the beam counter and in the ionization chamber. The ratio of the counts in the muon-monitor telescopes to the counts in the beam counter demonstrated the stability of f_π as a function of time. Table V summarizes the variation of the ratio of the muon-monitor scalers to the beam-counter scalers.

3. *Number of protons*

To find the net number of protons (N_p) after the target-empty subtraction, notice was taken of two effects. First, the data analysis accepted events from a region 10 cm long and centered on the liquid cell. Thus the target-full sample included events from the H_2 gas envelope. Second, for the target-empty runs, the target was not evacuated, but remained full of cold H_2 gas. During the target-empty runs, the temperature of the gas in the ballast vessel, as well as the gas in the target, was higher than that which prevailed in the presence of the liquid. The gas within the accepted volume with the target-full added 3% to the effective target thickness. With the target empty, the warmer H_2 gas that remained in the full 10-cm fiducial volume also amounted to 3% of the LH_2 in the cell. These factors canceled to 0.1%, with a systematic

TABLE IV. Determination of the fraction of the beam that was pions. The notation n, r, or u means normal, reverse, or undetermined chopper polarity. f_π^B is the value at the beam counter determined from the chopper data and f_π^{PH} is the corresponding value from the beam-counter pulse height.

T_π (MeV)	Polarity	Beam tune	f_π^n	f_π^r	f_π^u	f_π^B	f_π^{PH}	Correction factor to target	f_π
90	+	Normal			0.854	0.844±0.030		0.954	0.805±0.029
90	−	Normal			0.753	0.732±0.100		0.953	0.698±0.095
70	+	Normal			0.778	0.761±0.068		0.953	0.725±0.065
70	−	Normal			0.565	0.553±0.145		0.951	0.526±0.138
50	+	Normal			0.588	0.572±0.113		0.948	0.542±0.107
50	−	Normal	0.482	0.339		0.410±0.072	0.381±0.028	0.947	0.365±0.026
30	+	Normal	0.354	0.268		0.311±0.045	0.296±0.020	0.938	0.280±0.017
30	+	Degrader	0.647	0.663		0.655±0.016	0.657±0.020	0.938	0.615±0.012
30	−	Degrader	0.597	0.551		0.574±0.024	0.553±0.014	0.937	0.525±0.009
30	−	Degrader, double intensity	0.639	0.677		0.658±0.019	0.639±0.012	0.937	0.603±0.009

TABLE V. Stability of the muon-monitor counts to the beam-counter counts and tabulation of the total angle-dependent systematic uncertainty of the data set from all sources.

T_π (MeV)	Polarity	Beam tune	Variation of beam monitors σ (%)	Systematic uncertainty of data at 50° (%)	100° (%)	150° (%)
90	+	Normal	0.4	0.8	0.7	0.7
90	−	Normal	1.7	1.4	2.2	4.8
70	+	Normal	0.8	0.8	0.9	0.9
70	−	Normal	2.0	1.0	1.1	3.9
50	+	Normal	1.2	1.2	1.0	0.9
50	−	Normal	1.5	1.2	2.3	5.2
30	+	Normal	2.0	2.6	1.6	1.2
30	+	Degrader	0.7			
30	−	Degrader	1.2	2.8	2.5	2.3
30	−	Double intensity	0.2			

uncertainty of 1.5% of the target thickness. Thus, N_p was obtained to good accuracy from just the thickness of the liquid target and its measured density.

The target thickness was also measured by using the differential range telescope located downstream of the H_2 target. At 30 MeV, with a 0.1% momentum bite in the pion channel and with the target full, enough CH_2 absorber was placed downstream of the target and upstream of the range telescope to bring the pions in the beam to rest within the telescope. The stopping distribution occupied roughly three counters in the telescope; the centroid of the distribution could be located by peak fitting to within 1% of a counter thickness. The target was then emptied and stabilized. Al foil was added to bring the centroid of the stopping distribution back to its target-full position. The method proved to be very sensitive; addition of 0.002 cm of Al caused a reproducible shift of the centroid.

A thickness of 0.160 ± 0.002 cm of Al was found to compensate for the difference in H_2 between target-full and target-empty. However, this measured the gas within the total length of the target and not just that within the accepted region. We estimate that the cold gas seen by the residual range measurement was 15% of the total target thickness. Approximately $\frac{2}{3}$ of this was subtracted out during the target-empty measurement. The systematic uncertainty of these numbers totaled 3% of the target thickness, so the range measurement could not be used to determine the absolute target thickness to better than 3%. Using the ratio of energy loss for 30-MeV pions in Al to that in H_2, we determined the effective thickness of the H_2 target was 0.160 ± 0.005 g/cm^2.

The differential range measurement was repeated many times during the experiment. The thickness of H_2 remained constant except for one occasion in the middle of data taking when H_2 was released from the system. As discussed previously (Sec. II C 1), the hydrostatic head of the liquid bulged the liquid cell and the level of the hydrostatic head was determined by the amount of H_2 in the closed system. Range measurements showed that the target lost (4 ± 1)% of its thickness at that time and remained stable at its new value thereafter. This corresponded to a 0.061-cm difference in the bulge.

The most direct determination of the target thickness was made after the run when the target was no longer surrounded by the rest of the apparatus and could be surveyed by a pair of autocollimated transits. The thickness of the liquid cell, including the bulge, was measured as a function of the liquid level in the target and the reservoir. In order to check the reproducibility of the bulge, the survey was performed twice with a complete warmup between observations. The results were the same to 0.01 cm. These measurements showed an approximately linear increase of the bulge as a function of liquid level. From sensors that detected the level of liquid in the reservoir, we found that the total bulge must have been between 0.071 and 0.178 cm out of a target-empty thickness of 1.425 cm. The most probable value for the bulge was 0.099 cm, so the thickness of the target was $1.524^{+0.079}_{-0.027}$ cm. After accounting for the 45° rotation of the target with respect to the beam and using the density of LH_2, we obtain a target thickness of $0.154^{+0.008}_{-0.003}$ g/cm^2 of H_2 (full width). This is reasonably consistent with the value obtained from the differential range measurements described above.

Folding the measurements and uncertainties together, we deduce that N_p during the 30-MeV π^+ and π^- runs and during the 50-MeV π^- run was 0.921×10^{23} atoms/cm^2 while for the rest of the data set it was 0.958×10^{23} atoms/cm^2. The uncertainty in N_p is ±3%.

IV. RESULTS AND DISCUSSION

Before giving the final differential cross sections, we summarize the systematic uncertainties and discuss several tests of both the relative cross sections and the absolute normalization.

A. Summary of systematic uncertainties

The last three columns of Table V summarize the systematic uncertainty in the angular distributions as a function of angle. The entries combine the contribution due to

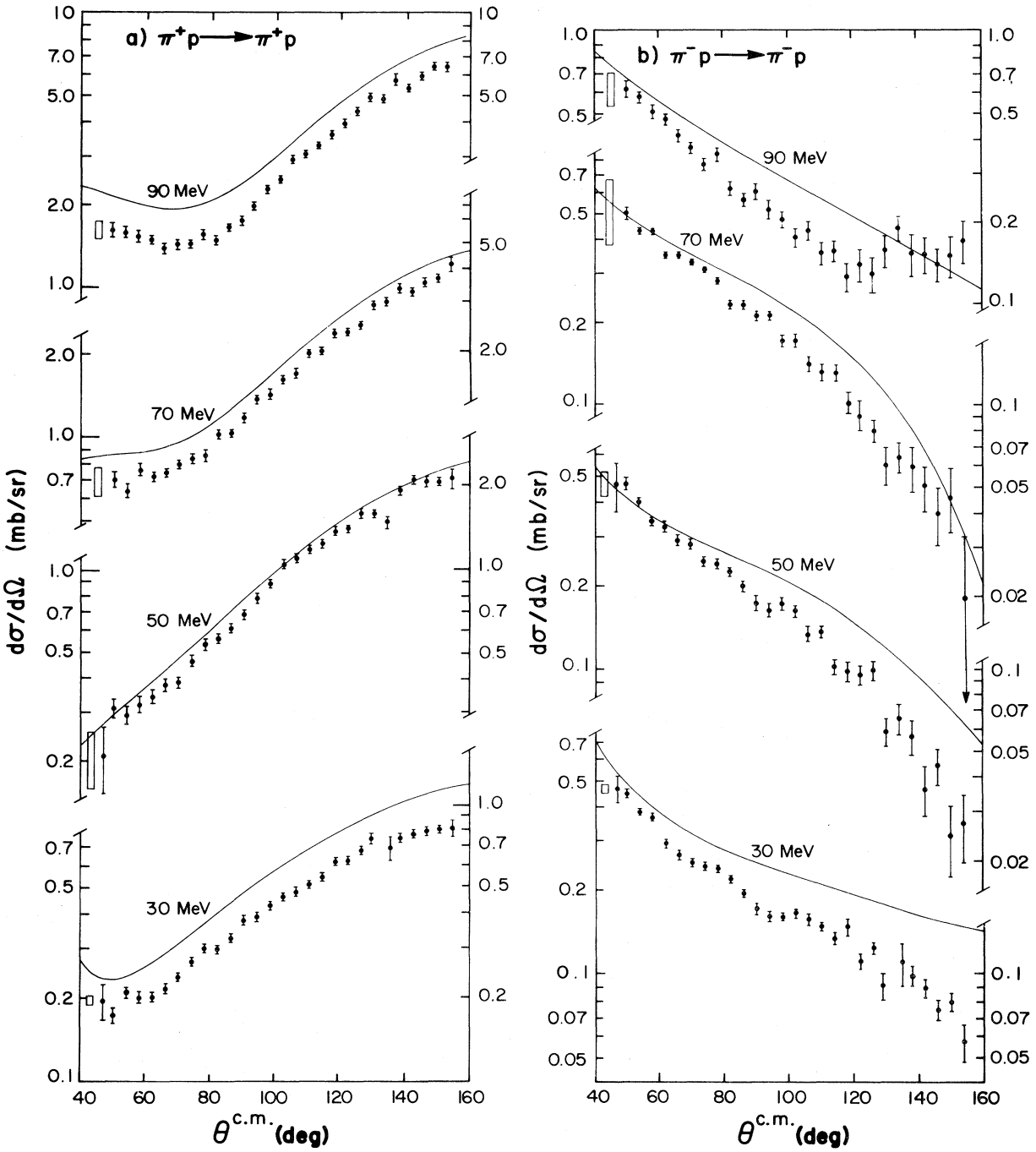

FIG. 9. Differential cross sections with statistical errors for this data set. (a) π^+p elastic scattering; (b) π^-p elastic scattering. The curves are from a phase-shift solution (Ref. 4) not including these data. The height of the rectangles to the left of each data set represents the 68% confidence interval of the normalizations.

the uncertainty in the time stability of f_π (derived from the variation of beam monitors also given in Table V) with systematic errors due to interaction corrections, absolute position uncertainties, electron contamination, and target-empty systematics. There is no reason to expect that the contributions from these different effects are correlated; the errors have been added in quadrature.

At 30 MeV, the interaction corrections dominate the systematic uncertainty. For backward π^-p scattering, the uncertainties in the elimination of backgrounds dominate the error. For all other data, the angle-dependent systematic error is less than 2%. For the entire data set, the systematic angular-dependent uncertainties are small compared to the statistical errors.

TABLE VI. Differential cross sections for $\pi^{\pm}p$ elastic scattering. The uncertainties are 1σ for normalization (N), statistical (stat), and systematic (syst) errors.

	T_π=29.4 MeV	
	π^+p	π^-p
	($N=\pm3.7\%$)	($N=\pm3.5\%$)
$\theta^{\text{c.m.}}$ (deg)	$d\sigma/d\Omega\pm$stat(syst) (mb/sr)	$d\sigma/d\Omega\pm$stat(syst) (mb/sr)
47	0.196±0.031(0.005)	0.465±0.058(0.013)
50	0.173±0.013(0.004)	0.446±0.017(0.012)
54	0.210±0.012(0.005)	0.380±0.013(0.011)
58	0.201±0.011(0.005)	0.363±0.013(0.010)
62	0.202±0.011(0.005)	0.292±0.013(0.008)
66	0.217±0.011(0.006)	0.266±0.013(0.007)
70	0.237±0.010(0.006)	0.249±0.013(0.007)
74	0.270±0.012(0.007)	0.242±0.009(0.007)
78	0.301±0.014(0.008)	0.238±0.009(0.007)
82	0.299±0.010(0.005)	0.218±0.007(0.005)
86	0.330±0.012(0.005)	0.194±0.008(0.005)
90	0.381±0.016(0.006)	0.170±0.010(0.004)
94	0.391±0.016(0.006)	0.160±0.009(0.004)
98	0.431±0.015(0.007)	0.159±0.007(0.004)
102	0.465±0.016(0.007)	0.164±0.008(0.004)
106	0.485±0.019(0.008)	0.156±0.009(0.004)
110	0.516±0.016(0.008)	0.147±0.007(0.004)
114	0.546±0.021(0.009)	0.133±0.008(0.003)
118	0.621±0.026(0.007)	0.147±0.012(0.003)
122	0.628±0.023(0.008)	0.110±0.008(0.003)
126	0.683±0.025(0.008)	0.123±0.007(0.003)
129	0.753±0.040(0.009)	0.091±0.011(0.002)
135	0.697±0.078(0.008)	0.109±0.020(0.003)
138	0.756±0.029(0.009)	0.098±0.009(0.002)
142	0.784±0.029(0.009)	0.089±0.008(0.002)
146	0.802±0.032(0.010)	0.074±0.007(0.002)
150	0.817±0.031(0.010)	0.079±0.007(0.002)
154	0.830±0.065(0.010)	0.057±0.009(0.002)

B. Comparison of data sets as a check on systematics

During the course of acquiring the data, several checks on its self-consistency were conducted. The results of these studies are summarized below.

(1) For one of the two detector rotations, the region at about 100° was observed by two sets of counters on opposite sides of the beam line. The two sets gave values consistent within statistics. The difference was (3±4)%.

(2) The differential cross sections obtained from the two rotations of the detector for each combination of energy and polarity gave consistent results. The χ^2 per degree of freedom (DF) for the difference between the two rotations typically had values near 1.0. The largest disagreement was for the π^-p scattering data at 30 MeV, where $\chi^2/\text{DF}=35.5/26$. This corresponds to a confidence level of about 10%. No dependence on scattering angle was found in the comparison between rotations. The difference in normalization of the two data sets was (1.0±1.1)%.

(3) Since the 30-MeV data were taken with two different beam conditions, we have calculated the results for each data set separately. The angular distributions for the two 30-MeV π^+ beams agreed within statistics. The difference in results was (6.2±1.7)% while the normalization error due to the combined uncertainties in f_π had a value of ±6.7%. For the two 30-MeV π^- data sets, the difference in results was (1.8±2.2)% and independent of scattering angle. The combined uncertainty in the normalization of these data from the uncertainties in f_π totaled ±2.4%. Since the results from the two beam tunes were consistent, the two data sets have been combined.

C. Checks of absolute normalization

Several checks have been made on the absolute normalization of this experiment. These fall into two categories: possible losses of data before taping and errors in analysis or simulation of the experiment.

1. Possible losses of data before taping

It is possible that systematic errors in the data acquisition could be responsible for a loss in signal. Several checks of possible losses due to trigger systematics were

TABLE VI. (*Continued.*)

$\theta^{c.m.}$ (deg)	T_π=49.5 MeV π^+p ($N=\pm 20.3\%$) $d\sigma/d\Omega\pm$stat(syst) (mb/sr)	π^-p ($N=\pm 7.8\%$) $d\sigma/d\Omega\pm$stat(syst) (mb/sr)
47	0.210±0.059(0.003)	0.463±0.098(0.005)
50	0.311±0.028(0.004)	0.467±0.026(0.005)
54	0.294±0.026(0.004)	0.399±0.019(0.005)
58	0.321±0.025(0.004)	0.341±0.015(0.004)
62	0.341±0.021(0.004)	0.324±0.015(0.004)
66	0.378±0.024(0.005)	0.290±0.014(0.003)
70	0.387±0.021(0.005)	0.280±0.012(0.003)
74	0.462±0.028(0.006)	0.243±0.011(0.003)
78	0.533±0.030(0.006)	0.238±0.011(0.003)
82	0.558±0.024(0.006)	0.223±0.009(0.005)
86	0.608±0.027(0.006)	0.197±0.009(0.004)
90	0.683±0.034(0.007)	0.171±0.011(0.004)
94	0.784±0.039(0.008)	0.160±0.011(0.003)
98	0.886±0.041(0.009)	0.170±0.009(0.004)
102	1.051±0.041(0.011)	0.160±0.008(0.003)
106	1.101±0.050(0.011)	0.132±0.009(0.003)
110	1.185±0.044(0.012)	0.134±0.008(0.003)
114	1.239±0.055(0.012)	0.101±0.007(0.002)
118	1.380±0.059(0.012)	0.096±0.009(0.005)
122	1.405±0.058(0.013)	0.093±0.008(0.005)
126	1.598±0.085(0.014)	0.097±0.009(0.005)
130	1.591±0.071(0.014)	0.058±0.007(0.003)
134	1.485±0.090(0.013)	0.065±0.009(0.003)
138	1.942±0.086(0.017)	0.055±0.008(0.003)
142	2.125±0.085(0.019)	0.036±0.008(0.002)
146	2.086±0.102(0.019)	0.043±0.007(0.002)
150	2.090±0.092(0.019)	0.024±0.007(0.001)
154	2.152±0.192(0.019)	0.027±0.008(0.001)

performed. For example, the MWPC requirement in the trigger was removed. These runs gave 0.991±0.021 of the signal observed in the corresponding runs with the chamber requirements in the logic. The beam counter was removed from the trigger logic for a π^+p run at 30 MeV. This run gave 0.995±0.050 of the results found with the normal trigger. In addition, at 50 MeV, runs were taken in which 2-ns timing changes were made to the beam counter to check possible timing errors. For these runs, the signal level was 0.976±0.015 of the normal 50-MeV π^-p runs. A more definitive test to check for timing problems was made by comparing the final results for events that projected into the half of the scintillation counters closer to the light pipes to the events that projected away from the light pipes. No discrepancy was found for any individual data set. The difference was (0.7±0.5)% for all the π^+ data.

During accumulation of the 90-MeV π^-p data, the trigger was changed from a three-counter coincidence to a two-out-of-three requirement. After analysis, but before interaction corrections, this run had (2.8±2.5)% less signal than the normal data run. We estimate a 0.5% difference in the interaction correction since no dE/dx requirements were applied for the 90-MeV data set; the agreement is within statistics.

The number of pions was determined by finding f_π in calibration runs and multiplying this number by the beam-counter scaler during data taking. The assumptions made in this technique have been discussed in Sec. III C 2. In addition, the accuracy of the beam-counter scaler was essential to give the absolute number of particles in the beam. Comparison of this scaler to another scaler controlled by different gates gave the dead time of the electronics. This dead time, which was typically 5%, was checked with other scalers. For some special runs, the beam counter was the only requirement of the trigger. For these runs, the beam-counter scaler that counted only during the live time was directly compared with the number of events that were written on magnetic tape. This checked both the beam-counter scaler and the data acquisition system under extreme conditions. We found that the number of events on magnetic tape was 0.980±0.013 of the beam-counter scaler. Here the error comes from the variance of several different runs. We believe the difference between this ratio and unity was due to higher-order corrections that were dead-time dependent. Since

TABLE VI. (*Continued.*)

	$T_\pi = 69.6$ MeV	
	π^+p	π^-p
	($N = \pm 9.5\%$)	($N = \pm 25.3\%$)
$\theta^{\text{c.m.}}$ (deg)	$d\sigma/d\Omega \pm$stat(syst) (mb/sr)	$d\sigma/d\Omega \pm$stat(syst) (mb/sr)
50	0.697±0.054(0.006)	0.504±0.030(0.005)
54	0.634±0.040(0.005)	0.435±0.018(0.004)
58	0.754±0.042(0.006)	0.432±0.017(0.004)
62	0.712±0.031(0.006)	0.352±0.015(0.004)
66	0.735±0.032(0.006)	0.352±0.018(0.004)
70	0.785±0.031(0.006)	0.330±0.015(0.003)
74	0.824±0.038(0.007)	0.310±0.012(0.003)
78	0.850±0.045(0.007)	0.289±0.012(0.003)
82	1.015±0.038(0.009)	0.234±0.011(0.003)
86	1.027±0.034(0.009)	0.230±0.010(0.003)
90	1.166±0.041(0.010)	0.217±0.014(0.002)
94	1.352±0.046(0.012)	0.211±0.014(0.002)
98	1.405±0.060(0.013)	0.179±0.011(0.002)
102	1.595±0.047(0.014)	0.177±0.010(0.002)
106	1.677±0.068(0.015)	0.148±0.011(0.002)
110	1.983±0.061(0.018)	0.132±0.010(0.002)
114	2.023±0.067(0.018)	0.132±0.009(0.002)
118	2.336±0.079(0.021)	0.103±0.011(0.004)
122	2.370±0.075(0.021)	0.094±0.011(0.004)
126	2.494±0.068(0.022)	0.080±0.008(0.003)
130	2.943±0.116(0.026)	0.069±0.011(0.003)
134	3.030±0.113(0.027)	0.074±0.009(0.003)
138	3.385±0.144(0.030)	0.059±0.012(0.002)
142	3.281±0.110(0.030)	0.051±0.012(0.002)
146	3.539±0.143(0.032)	0.040±0.010(0.002)
150	3.666±0.161(0.033)	0.046±0.012(0.002)
154	4.135±0.281(0.037)	0.019±0.013(0.001)

the dead time was very large (>99%) for these runs and small (~5%) for the normal data, no significant correction or uncertainty is expected to apply to the normal data for events lost in the taping process.

2. *Possible analysis or simulation losses*

Several checks were made to ensure that the analysis code was performing as expected. The most complete was to check that no net signal was lost due to cuts that were applied in the analysis. Losses of net signal were small from the sample of events with too little or too much MWPC information to extract a track. These losses were typically ~0.2% and corrections for these effects have been included. The net signal from events that extrapolated outside of the counter, chamber, or target fiducial areas are understood since the same fiducial cuts were applied in the simulation as in the data analysis.

The Monte Carlo calculation of the solid angle was checked analytically for one counter. The agreement was good. Several changes were made to the analysis cuts that defined a scattered pion. These same changes were made to the cuts in the Monte Carlo. The differential cross sections remained unchanged.

D. Final results and discussion

The differential cross sections for π^+p elastic scattering are shown in Fig. 9 and are tabulated in Table VI. The errors that are plotted are statistical only and combine the data, target-empty subtraction, and Monte Carlo contributions. A separate tabulation of systematic uncertainties is also listed in Table VI. Since the systematic uncertainties are small compared to the statistical errors, these errors should be added in quadrature to give the uncertainties for any phase-shift analysis that does not deal with correlations between the systematic errors explicitly.

In addition the overall normalization uncertainties are tabulated. The uncertainties in normalization between data sets were obtained by combining the uncertainties due to f_π, N_p, and nonanalyzable events in quadrature. The uncertainty in N_p dominates the error for the 30-MeV data; the uncertainty in f_π dominates the normalization error for all other data. The normalization uncertainties for 30-MeV π^+p and π^-p are correlated since the dominant error comes from the uncertainty in N_p.

The differential cross sections are generally smooth for the entire data set. There is no obvious structure for the data beyond those allowed from the level of the systematic uncertainties as summarized in Table VI.

TABLE VI. (*Continued.*)

	$T_\pi = 89.6$ MeV	
	$\pi^+ p$ ($N = \pm 4.7\%$)	$\pi^- p$ ($N = \pm 13.9\%$)
$\theta^{\text{c.m.}}$ (deg)	$d\sigma/d\Omega \pm$stat(syst) (mb/sr)	$d\sigma/d\Omega \pm$stat(syst) (mb/sr)
50	1.616±0.121(0.013)	0.613±0.051(0.009)
54	1.579±0.077(0.013)	0.574±0.033(0.008)
58	1.523±0.087(0.012)	0.507±0.034(0.007)
62	1.480±0.066(0.012)	0.477±0.025(0.007)
66	1.378±0.068(0.011)	0.417±0.024(0.006)
70	1.420±0.068(0.011)	0.375±0.022(0.005)
74	1.421±0.061(0.011)	0.325±0.019(0.005)
78	1.544±0.079(0.012)	0.355±0.024(0.005)
82	1.460±0.066(0.010)	0.267±0.017(0.006)
86	1.634±0.060(0.011)	0.243±0.015(0.005)
90	1.728±0.081(0.012)	0.260±0.020(0.006)
94	1.957±0.094(0.014)	0.224±0.021(0.005)
98	2.249±0.096(0.016)	0.205±0.017(0.005)
102	2.435±0.084(0.017)	0.176±0.015(0.004)
106	2.875±0.120(0.020)	0.187±0.017(0.004)
110	3.010±0.108(0.021)	0.155±0.016(0.003)
114	3.235±0.101(0.023)	0.157±0.016(0.003)
118	3.526±0.152(0.025)	0.127±0.017(0.006)
122	3.878±0.156(0.027)	0.140±0.020(0.007)
126	4.309±0.156(0.030)	0.130±0.020(0.006)
130	4.814±0.164(0.034)	0.159±0.023(0.008)
134	4.726±0.149(0.033)	0.192±0.022(0.009)
138	5.568±0.317(0.039)	0.154±0.028(0.008)
142	5.197±0.210(0.036)	0.153±0.025(0.008)
146	5.764±0.237(0.040)	0.141±0.021(0.007)
150	6.215±0.195(0.044)	0.152±0.027(0.007)
154	6.216±0.311(0.044)	0.172±0.032(0.008)

The curves that appear on the plot are obtained from the energy-dependent phase-shift solution for 0 to 350 MeV from the VPI group.[4] They do not include the effect of this data set on the fit. At these low energies, the phase-shift predictions for $\pi^+ p$ scattering from the Karlsruhe collaboration[10] differ by no more than 10% from those of the VPI group.

Apart from normalization differences, the cross sections we obtain for $\pi^+ p$ elastic scattering are fairly consistent with predictions from the phase-shift solutions. At 90 MeV, the forward-angle $\pi^+ p$ data lie further below the prediction than do the backward-angle data. For $\pi^- p$ elastic scattering, however, there are substantial differences in shape. This is not disturbing, since there are very few existing low-energy $\pi^- p$ elastic scattering data.

The absolute values of the cross sections from this experiment are lower than phase-shift predictions by approximately 20% at 90-MeV $\pi^+ p$ scattering and by 25% at 30-MeV $\pi^+ p$ scattering. The same phase-shift solution agrees reasonably well with the Bussey *et al.*[6] and the Bertin *et al*[7] data. At the other $\pi^+ p$ energies, the uncertainty of the normalization of our results is large and we find no significant difference in normalization. For forward-angle $\pi^- p$ scattering, the normalization of the phase-shift predictions and this data set is the same to within our uncertainty.

It is hard to reconcile the normalization discrepancies between our cross sections and previous data. The checks we have made on the trigger logic, the data acquisition system, and the analysis convince us that no significant losses occurred to the scattered-pion signal. We believe the uncertainties that we assign to the incoming pion flux and the effective number of protons in the target are realistic. At 90 MeV, conservative assumptions were made to determine the uncertainty of the number of pions based upon measurements of the beam composition and about the stability of the effective number of protons in the target as a function of time. For both $\pi^+ p$ and $\pi^- p$ at 30 MeV, we feel most confident of the absolute normalization, since many checks on the target thickness were interleaved with these data and redundant measurements of the pion beam flux were made at 30 MeV.

We do not publish our own set of phase-shift solutions for these data. However, the main effect of our data on the phase-shift solutions will be to make the low-energy phase shift in the isospin-$\frac{1}{2}$ channel more precisely determined. Our data will tend to decrease the S_{11} phases and make the S_{31} phases more negative at low energy.

ACKNOWLEDGMENTS

We wish to express our appreciation to the LAMPF staff for providing support for this experiment. We thank V. Armijo, C. Dalton, G. Krausse, F. Montoya, F. Ribe, and T. Sandford for technical support. We appreciate the engineering support from R. Harrison and R. Damjanovitch and thank J. Novak for providing the H_2 target. Thanks also go to S. Johnson and M. Hudson for help with the data analysis. We appreciate the help of D. Dodder from Los Alamos and from R. Arndt and D. Roper from VPI for their phase-shift predictions. This work was supported by the U.S. Department of Energy.

---

*Present address: Department of Physics, Massachusetts Institute of Technology, Cambridge, MA 02139.

[1]See R. J. McLeod and D. J. Ernst, Phys. Rev. C 23, 1660 (1981); C. Coronis and R. H. Landau *ibid.* 24, 605 (1981); and references therein.

[2]See, for example, M. K. Banerjee and J. B. Cammarata, Phys. Rev. C 17, 1125 (1978); G. Resele and C. Schmid, Phys. Rev. D 22, 121 (1980); S. Morioka and I. R. Afnan, Phys. Rev. C 26, 1148 (1982).

[3]C. A. Dominguez and P. Langacker, Phys. Rev. D 24, 1905 (1981).

[4]For a list of references to the data of the π-nucleon system, see V. S. Zidell, R. A. Arndt, and L. D. Roper, Phys. Rev. D 21, 1255 (1980). The phase-shift solution CP350, generated from their program SAID, was used to compare our data with the results of other experiments.

[5]E. G. Auld, D. Axen, J. Beveridge, C. Duesdieker, L. Felawka, C. H. Q. Ingram, R. R. Johnson, G. Jones, D. LePatourel, R. Orth, M. Salomon, W. Westlund, and L. P. Robertson, Can. J. Phys. 57, 73 (1979).

[6]P. J. Bussey, J. R. Carter, D. R. Dance, D. V. Bugg, A. A. Carter, and A. M. Smith, Nucl. Phys. B58, 363 (1973).

[7]P. Y. Bertin, B. Coupat, A. Hivernat, D. B. Isabelle, J. Duclos, A. Gerard, J. Miller, J. Morgenstern, J. Picard, P. Vernin, and R. Powers, Nucl. Phys. B106, 341 (1976).

[8]LeCroy Research Systems, Spring Valley, New York, 10977.

[9]C. G. Dalton, Los Alamos National Laboratory Report No. LA-7143, 1978 (unpublished).

[10]G. Höhler, F. Kaiser, R. Koch, and E. Pietarinen, *Handbook of Pion-Nucleon Scattering,* Physics Data No. 12-1 (Fachsinformationszentrum, Karlsruhe, 1979).